Phase signal analysis for high-sensitive temperature fiber-optic external Fabry-Perot-cavity sensor

T. Lozano-Hernandez[a,*], D. Jauregui-Vazquez[b], J. M. Estudillo-Ayala[a], E. Diaz-Cervantes[c], J. A. Alvarez-Chavez[d], J. M. Sierra-Hernandez[a], and H. L. Offerhaus[c]

[a]*Departamento de Ingeniería Electrónica, División de Ingenierías Campus Irapuato Salamanca, Universidad de Guanajuato, Carretera Salamanca-Valle de Santiago km 3.5 + 1.8 km, Salamanca, Gto., 36885, México.*
[b]*Centro de Investigación Científica y de Educación Superior de Ensenada, División de Física Aplicada-Departamento de Óptica, Carretera Ensenada-Tijuana, No. 3918, Zona Playitas, Ensenada 22860, BC, México.*
[c]*Departamento de Alimentos, Centro Interdisciplinario del Noreste, Universidad de Guanajuato, 37975 Tierra Blanca, Guanajuato, México,*
[4]*Optical Sciences Group - University of Twente, Drienerlolaan 5, 7522 NB, Enschede, The Netherlands.*

Received 28 July 2023; accepted 93 April 2024

We experimentally demonstrate a highly temperature-sensitive external Fabry-Perot cavity. The interferometric structure is composed of an air-microcavity; its fabrication uses a microcapillary and UV polymer. A temperature sensitivity close to 5.7 nm/°C is achieved with suitable linearity (0.9896) and minimal hysteresis; a phase analysis technique is proposed and applied to overcome the trade-off between sensitivity and range of operation. This technique provides a competitive sensitivity (0.84 rad/°C), good linearity (0.9934), and a range of operation from 25°C to 41°C.

Keywords: Fabry-Perot interferometer; optical fiber sensor; temperature measurement; phase signal analysis; polymer.

DOI: https://doi.org/10.31349/RevMexFis.70.051302

1. Introduction

External Fabry Perot Interferometers (EFPI) have been investigated for several decades [1-3]. Temperature measurement is one of the first and most attractive applications [1,4]. With the arrival of UV-cured polymers, the fabrication of these devices turned cost-effective and straightforward. Often this cavity is generated at the tip of optical fibers, creating a probe for temperature and refractive index [5]. The polymer microcavity can also be created inside an optical fiber for simultaneous detection of humidity and temperature [6,7]; Furthermore, the sensor's performance can be improved using a Fiber Bragg Grating (FBG) for simultaneous detection of some parameters [8,9]. UV-cured polymers have been used to improve the sensitivity of some Mach-Zehnder interferometers [10]. The most commonly used implementation employs silica capillary tubes [11-16]. A fiber is inserted into the capillary, and the fiber is fixed using the UV polymer. Another optical fiber is set on the opposite side. Such configurations present high sensitivity to parameters such as curvature [17], strain [18], and temperature [16]. The high sensitivity implies measurement limited unambiguous measurement range. This trade-off can be overcome by phase analysis [19,20]. In this work, an External Fabry Perot Interferometer is fabricated and operated with phase analysis. The optical fiber structure represents a reliable alternative to measure temperature in applications related to room temperature.

This work aims to demonstrate that by the phase signal analysis technique, it is possible to attend to the following challenges: avoiding the trade-off when two measurements overlap due to the phase analysis do not consider the wavelength reference points. Furthermore, by this technique, the dynamic range of the sensor can be increased due to the phase of the interferometric signal that can be measured beyond the wavelength range. These features are described in detail below.

2. Fabrication process

Figure 1 shows the manufacturing route of the Capillary Low-coherence External Fabry-Perot Interferometer (CLEFPI). A single-mode fiber (630-HP) is cleaned and cleaved; then, it is aligned to a 1 μL capillary [Fig. 1a)] using a 3D translation (MBT610D). The capillary has a 200 μm inner diameter and a total length of 3.2 cm. The optical fiber is inserted halfway into the capillary using the translation stage, and a sensitive UV glue polymer is applied at the end of the capillary [Fig. 1b)]. Then a second 630-HP fiber is introduced from the opposite side of the capillary. When a suitable cavity length is achieved (typically 7 microns), the glue is added and cured [Fig. 1c)]. The final optical fiber structure is presented in Fig. 1d). The cavity length L is controlled by the Z plane of the 3D translation stage. Moreover, the cavity losses are minimized by using the XY positions.

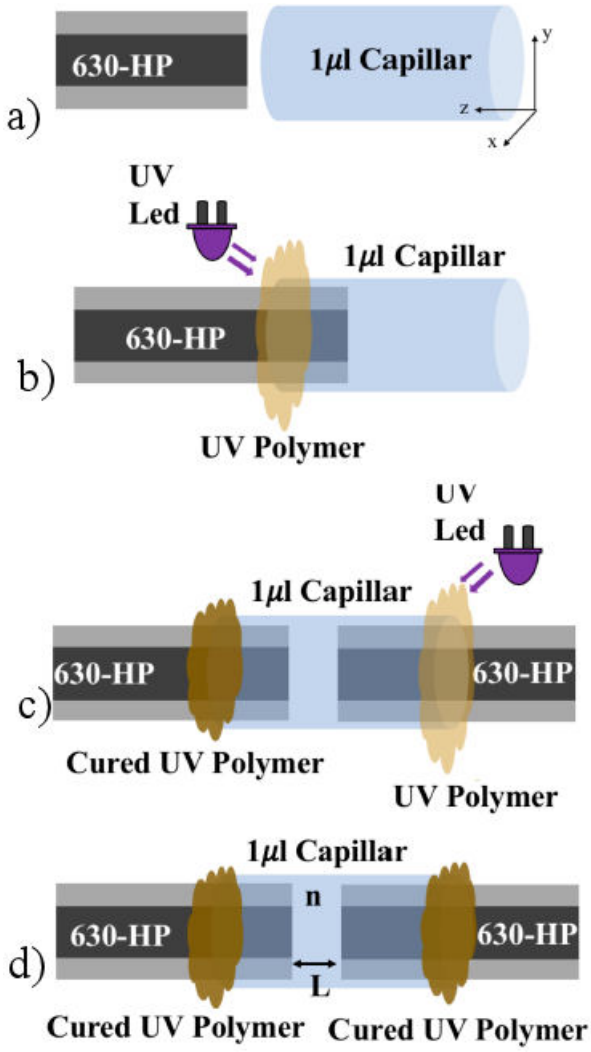

FIGURE 1. Fabrication procedure: a) prepare 1 μL capillary and 630-HP fiber, b) insert 630-HP fiber into one end of the 61 μL capillary and set by cured UV polymer, c) repeat the prosses at the opposite position to close the cavity by inserting the second 630-HP, and d) final cavity structure.

In Fig. 2, the cavity is shown. When the polymer is cured, an air microcavity is generated between the two flat ends of the fibers, the refractive index transitions are given by silica fiber $nf = 1.4570$ and air $n = 1.00$ that yield a reflectivity [21]:

$$\left|\frac{n_f - n}{n_f + n}\right|^2. \quad (1)$$

We assume that $R_1 = R_2 = R$. The cavity can be modeled as a one layer Fabry-Perot cavity which yields:

$$R(\lambda) = R + R(1-R)^2 + 2R(1-R)\cos(4\pi nL\lambda). \quad (2)$$

The phase-term at the right had side depends on the cavity refractive index n, the physical cavity length L, and the free space wavelength λ. Since the UV polymer is not inside the cavity, the polymer is not considered in the cavity reflections [22].

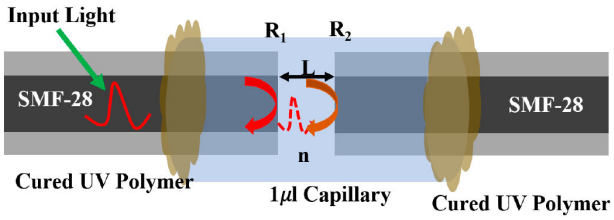

FIGURE 2. Sketch of Capillary Low-coherence External Fabry-Perot Interferometer.

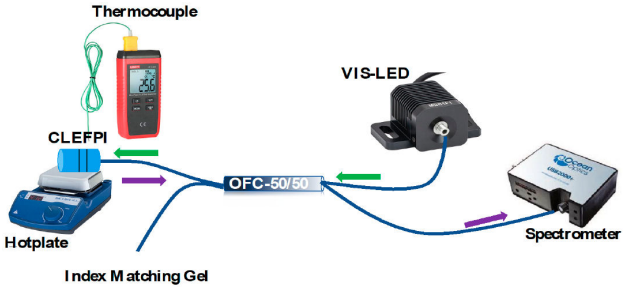

FIGURE 3. Experimental setup to characterize the CLEFPI.

3. Experimental setup

Figure 3 shows the light from a visible led (MBB1F1) is launched to the CLEFPI using a 2×2 optical fiber coupler (TW670R5A2). One output of the coupler is using an index matching gel, and the other port is connected to the CLEFPI. The reflected signal is monitored by the fourth port using spectrometer (2000+ UV-VIS) and computer.

Of the coupling between the single-mode 630-HP optical fiber (3.5μ) and the VIS-LED is low so that the VIS-LED is operated at maximal current (500 mA), while the integration time of the spectrometer is set at 50 msec.

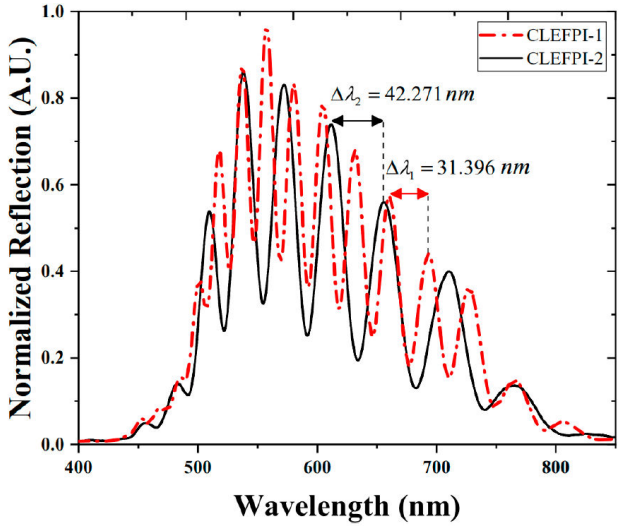

FIGURE 4. Interference spectrums of the fabricated CLEFPIs. CLEFPI-1 (dot line) and CLEFPI-2 (continuous line).

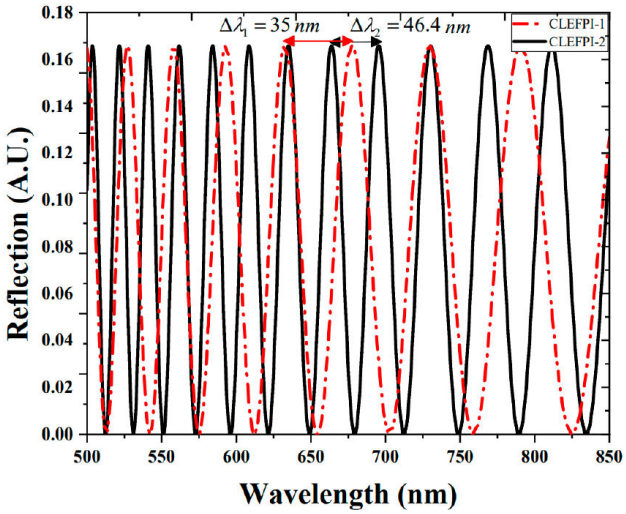

FIGURE 5. Interference spectrum response of the CLEFPIs considering the estimated cavity length.

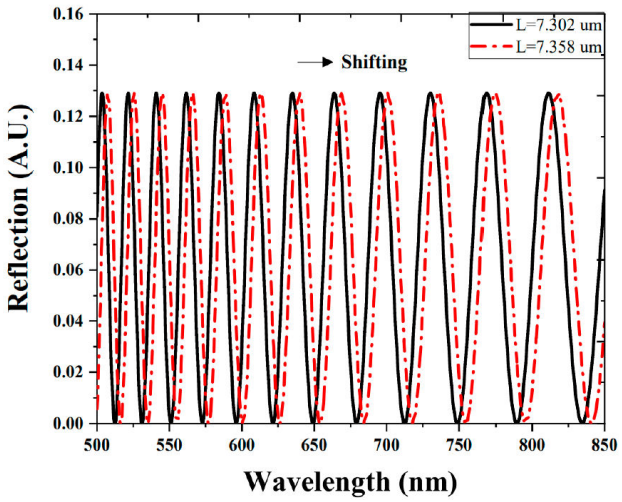

FIGURE 6. Reflection response as the CLEFPI cavity length is varied.

4. Principle of operation

To demonstrate the operation of the CLEFPI, the reflections spectra of CLEFPI-1 and CLEFPI-2 are shown in Fig. 4.

Figure 4, interference spectrums of the fabricated CLEFPIs. CLEFPI-1 (dot line) and CLEFPI-2 (continuous line).

The cavity length can be computed from the Free Spectral Range (FSR) shown in Fig. 4 as [23]:

$$FSR = \lambda_2 - \lambda_1 = \frac{\lambda_2 * \lambda_1}{2nL}, \tag{3}$$

where λ_1 and λ_2 represent the position of two consecutive peaks. These yields: CLEFPI-1=7.302 μm and CLEFPI-2=4.743 μm. Figure 5 shows a simulation of the reflectivites using these cavity lengths but ignoring the cavity losses.

The position of the minima can be described by [24]:

$$\lambda_d = \frac{2nL}{m}, \tag{4}$$

where the cavity refractive index n and length L are described above, and m is an integer. When the temperature is varied, the refractive index of the air does not change significantly. The UV polymer however, shows a linear expansion and as a result, the cavity length varies and the positions of the minima are shifted by:

$$\Delta\lambda_d = \frac{2n\Delta L}{m}. \tag{5}$$

The cavity length variation is related to the linear Thermo Expansion Coefficient (TEC-α-) as $\Delta L = \alpha\Delta T$. The wavelength shift can thus be expressed in terms of the temperature variations as [25]:

$$\Delta\lambda_d = \frac{\lambda_d\Delta L}{L} = \frac{\lambda_d\alpha\Delta T}{L}. \tag{6}$$

For CLEFPI-1 at 625 nm, a shift of 5 nm is appreciated; this wavelength shifting corresponds to a cavity length variation of 56 nm, where the position of the minima shifts to longer wavelengths as the temperature increases (see Fig. 6).

5. Temperature wavelength analysis

As shown in Fig. 3, the CLEFPI is located over a hot plate (C-MAG HP4) and a thermocouple (UT320D) is used to monitor the temperature at the location of the CLEFPI. The reflection signal was recorded at increments of 2°C for temperature increase and decrease. Both interferometers were evaluated, and their thermal response is shown in Fig. 7.

Sensitivities of 5.248 nm/°C (CLEFPI-1) and 5.773 nm/°C (CLEFPI-2) is achieved. The temperature range variation is limited by the ambiguity that arises from shifts over more than half an FSR. This interferometric structure exhibits sensitivity comparable to prior works based on polymer cavities (see Table I).

The adjusted square indicates good linearity for the temperature increment range from 25°C to 33°C (R-square

TABLE I. Comparative performance in terms of sensitivity and temperature range operation.

Sensitivity (nm/°C)	Range(°C) /step(°C)	Year	Ref.
0.48	25-45/5	2019	7
0.34	25-45/5	2020	8
0.19	25-55/5	2014	5
2.22	28-34/1	2021	26
2.46	2-35/1	2021	27
2.88	25-55/2	2020	16
5.2	15-22/1	2013	28
5.7	25-35/2	–	this work

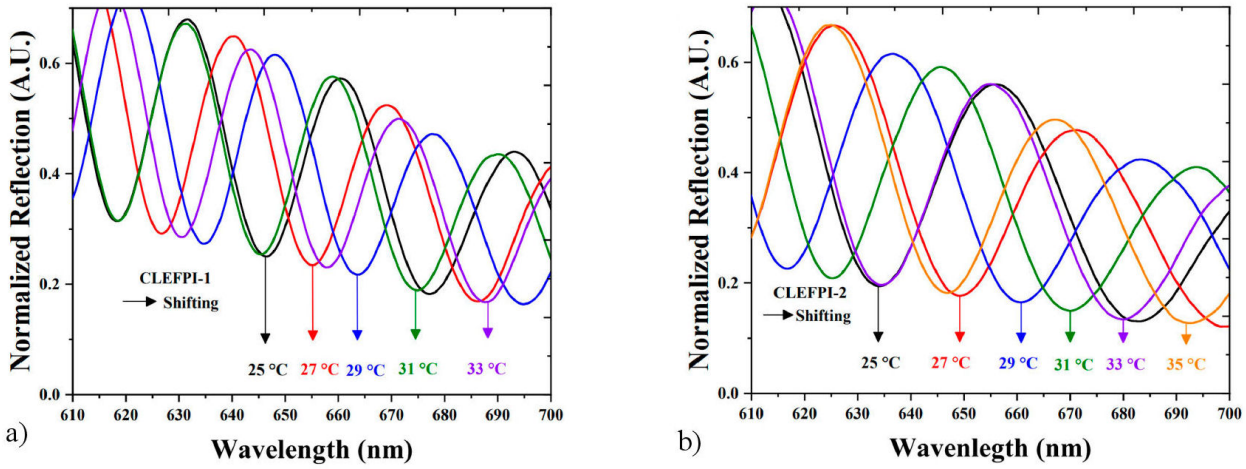

FIGURE 7. Thermal response of a) CLEFPI-1 and b) CLEFPI-2.

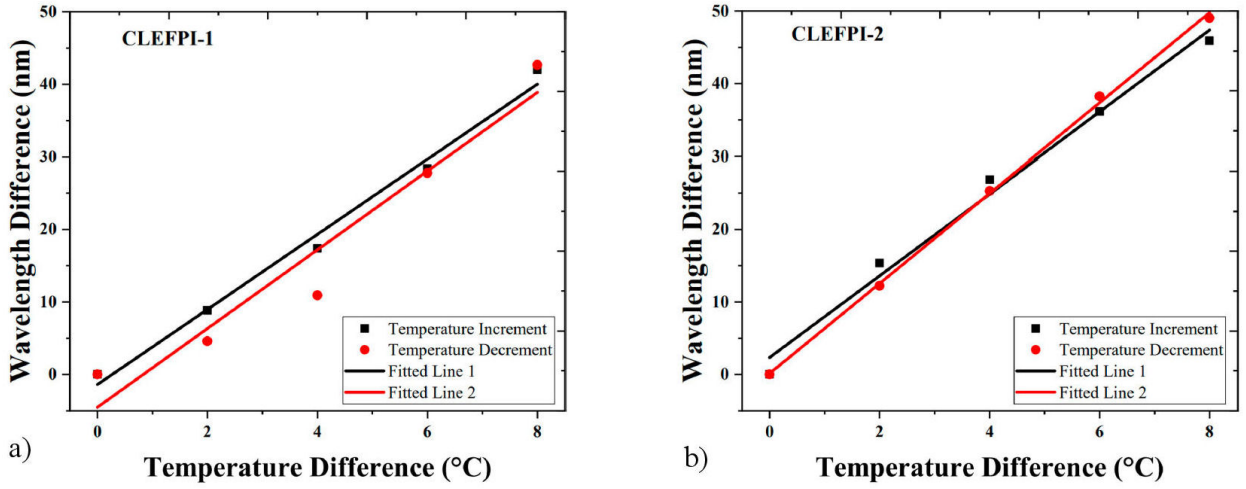

FIGURE 8. Hysteresis analyses of the a) CLEFPI-1 and b) CLEFPI- 2.

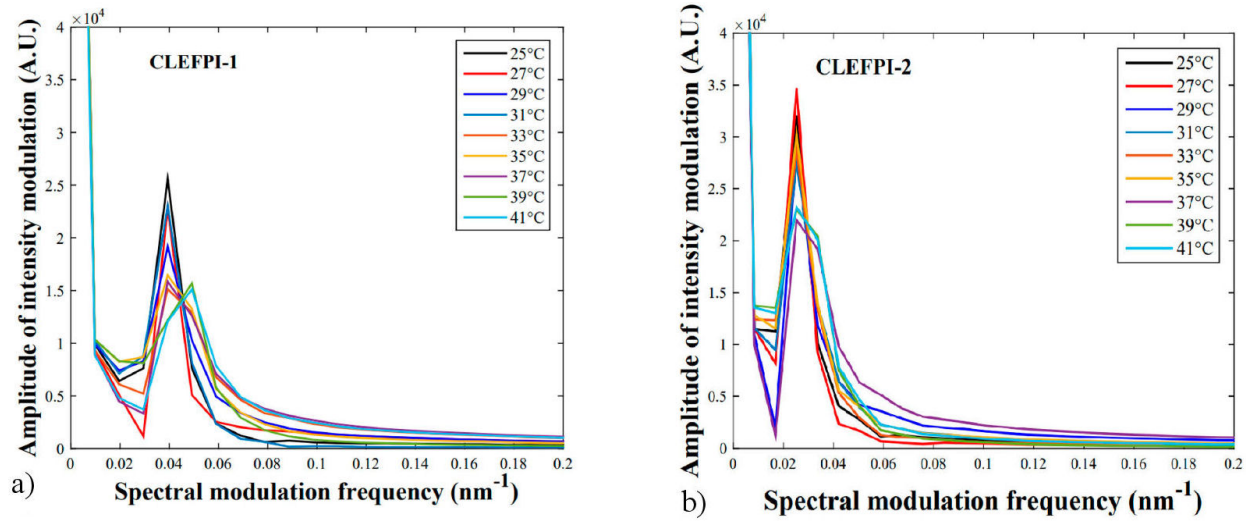

FIGURE 9. Spatial frequency spectrums of the interferences reflections signals of a) CLEFPI-1 and b) CLEFPI-2 for temperature ranges from 25°C to 41°C.

=0.98965 for CLEFPI-1 and R-square =0.98965 for CLEFPI-2). An analysis of the hysteresis is presented in Figure 8 and indicates minimal path difference in both interferometers and good reversibility. Although the fabricant does not provide information about the TEC, this value can be estimated by some optical techniques [29].

As shown in Fig. 7, the temperature range operation is limited by the FSR so that the same effect is detected at 33°C and 27°C.

6. Accumulative phase signal analysis

As mentioned above, and paying particular attention to Fig. 7, the overlap measurement between the initial and final point limits the wavelength analysis; if the temperature range increases, other measurement values will also overlap, and consequently, the temperature range operation is limited. An accumulative phase method is proposed to remove the ambiguity and improve the range operation. The intensity reflection spectrum generated by Eq. (1) can be expressed as the Fourier spectrum by:

$$f(q) = \sum_{n=1,M} e^{iq\lambda_n} R(\lambda_n). \tag{7}$$

By using the positive q data from the complex Fourier signal, it is possible to obtain the total phase from the interference spectrum [19,30]. The Fourier spectrums of the interference signals shown in Fig. 7 are depicted in Fig. 9.

The spatial frequency spectrums show a DC component, centered 0 nm^{-1}, and an intensity peak component. Here, we consider the regions with symmetric FSR. The phase is extracted from the spatial frequency components that is at centered 5 nm^{-1} (CLEFPI-1) and 3 nm^{-1} (CLEFPI-1). The phase generated by the temperature changes is presented in Fig. 10. It can be observed that the phase increase as the temperature increase for the measurement ranges 25-29°C (CLEFPI-1) and 25-31°C (CLEFPI-2) the phase varies of 2/pi. In Fig. 10b) the phase has been unwrapped.

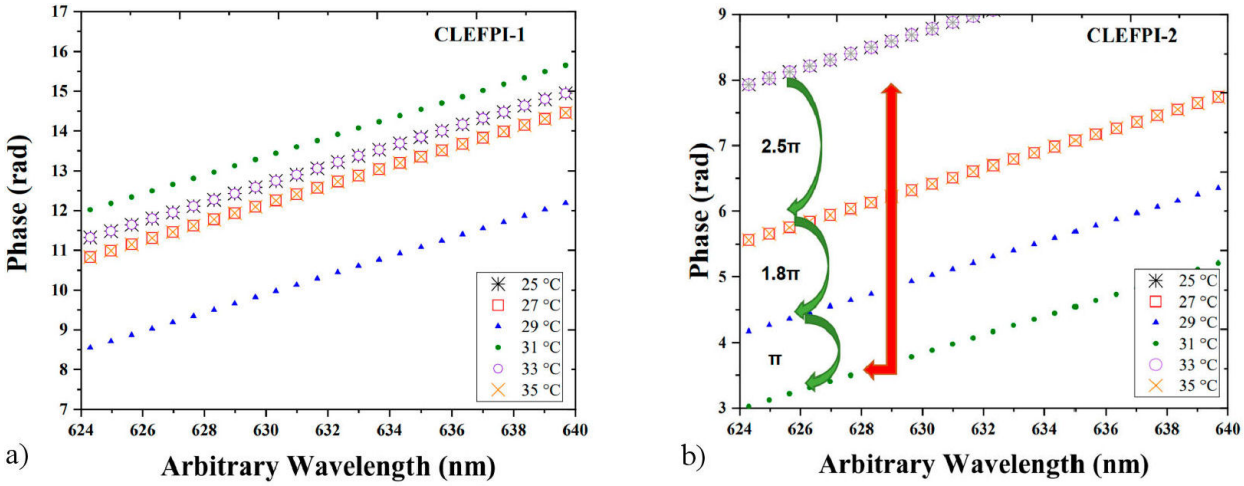

FIGURE 10. Phase-temperature variation for a) CLEFPI-1 and b) CLEFPI-2.

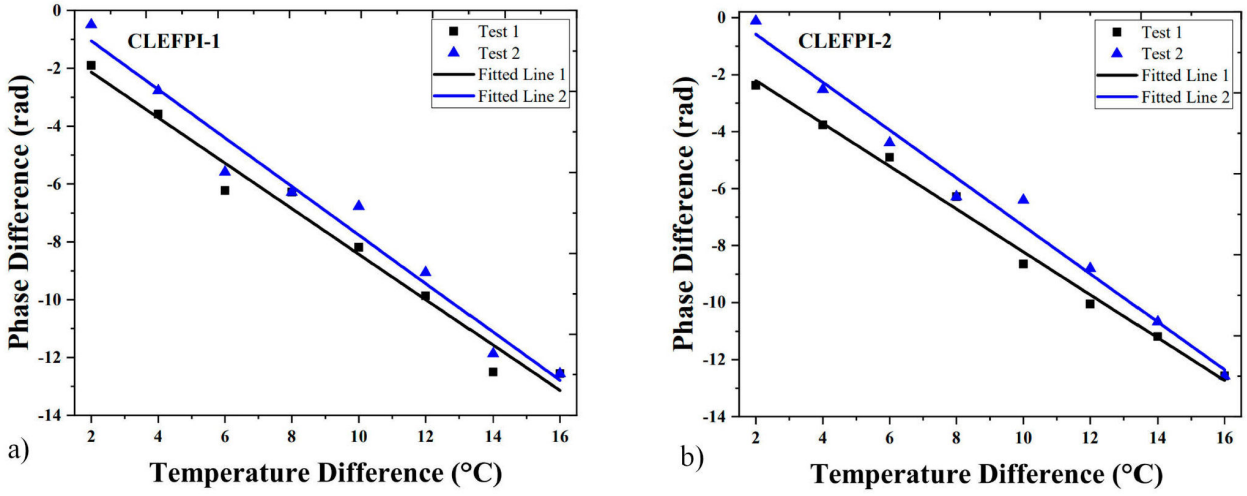

FIGURE 11. Phase sensitivity analysis of a) CLEFPI-1 and b) CLEFPI-2, after two consecutive rounds.

As can be appreciated in Fig. 10a), the phase of some measurements overlaps; this relates to the interference wavelength spectra, and its representation corresponds to the temperature values 25 and 33 in Fig. 7. However, by using this unwrapping, it is possible to estimate the total phase change as the temperature increases [see Fig. 10b)]; consequently, the trade-off measurement is avoided, and the temperature range increases. In Fig. 11, the phase response of CLEFPI-1 and CLEFPI-2 can be observed. Here, two tests were conducted to validate the method. As can be observed, both of them exhibit similar phase sensitivities -0.83rad/°C (CLEFPI-1) and -0.84rad/°C (CLEFPI-2). Furthermore, the linearity is competitive (R-square =0. 97575 for CLEFPI-1 and R-square =0. 99341 for CLEFPI-2); Moreover, according to Fig. 11, the phase extracted from the interference spectra was used to detect temperature without ambiguity points usually observed wavelength spectra and moreover it can be appreciated that the temperature range can be beyond initial temperature range analyzed. This technique can be applied at any highly sensitive interferometric device that provides phase modulation.

7. Conclusions

A high-sensitive temperature External Fabry-Perot interferometer is experimentally demonstrated and analyzed. A cured UV polymer composes the optical fiber structure. The linear Thermo Expansion Coefficient governs the temperature sensor operation and provides sensitivities close to 5.248 nm/°C (CLEFPI-1) and 5.773 nm/°C (CLEFPI-2) in the range from 25°C to 35°C. Considering the adjusted square (R2 =0.98965 for CLEFPI-1 and R2 =0.98965 for CLEFPI-2), the sensor presents good linearity, and moreover, the hysteresis analysis also indicates minimal path difference when the temperature follows the increase-decrease route. Despite the presented results being competitive compared to prior works, the results imply a challenge related to measurement overlap, limiting the temperature range operation. A phase signal analysis attends to this challenge. Hence, the phase is extracted from the peaks at Fourier spectrums. Then the total phase difference is computed in terms of the temperature variation. As a result, the following sensitivities were achieved: -0.83 rad/°C (CLEFPI-1) and -0.84 rad/°C (CLEFPI-1). The phase analyses avoid the measurement overlap and increase the temperature range operation (from 25°C to 41°C). Furthermore, the linearity is suitable for sensing applications (R2 = 0.97575 for CLEFPI-1 and R2 = 0.99341 for CLEFPI-2). The proposed structure implies a cost-effective implementation and can be used for monitoring bio-thermal changes.

Considering the temperature range operation and the sensitivity achieved, some future research directions can be human temperature and pressure monitoring as well as biological temperature monitoring, for instance, cell culture incubation and microbial fermentation where the ideal temperature range varies depending on the organism; however, this temperature often falls within the 25°C to 41°C range.

Acknowledgment

T. Lozano-Hernandez is grateful to CONAHCYT for the support under scholarship 777601/825870, University of Guanajuato and CIIC-UG 166/2023. This research was funded by CONAHCYT Grant A1-S-33363/CB2018.

1. C. E. Lee *et al.*, Optical-fiber Fabry-Perot embedded, sensor Opt. **14** (1989)
2. T. Li *et al.*, Optical scanning extrinsic Fabry-Perot interferometer for absolute microdisplacement measurement, Appl. Opt. **36** (1997)
3. Y. J. Rao, Recent progress in fiber-optic extrinsic Fabry-Perot interferometric sensors, Opt. Fiber Technol **12** (2006) 227-237
4. C. E. Lee and H. F. Taylor, Fiber-optic Fabry-Perot temperature sensor using a low-coherence light source, J. Light. Technol **9** (1993) 129
5. X. L. Tan *et al.*, UV-Curable Polymer Microhemisphere-Based Fiber-Optic Fabry-Perot Interferometer for Simultaneous Measurement of Refractive Index and Temperature, IEEE Photonics J. **6** (2014)
6. R. Oliveira, L. Bilro, and R. Nogueira, Fabry-Pérot cavities based on photopolymerizable resins for sensing applications, Opt. Mater. Express. **8** (2018)
7. A. G. Leal-Junior *et al.*, Analysis of viscoelastic properties influence on strain and temperature responses of Fabry-Perot cavities based on UV-curable resins, Opt. Laser Technol **120** (2019)
8. D. Yang *et al.*, Integrated optic-fiber sensor based on enclosed EFPI and structural phase-shift for discriminating measurement of temperature, pressure and RI, Opt. Laser Technol **126** (2020)
9. R. Oliveira *et al.*,, Simultaneous detection of humidity and temperature through an adhesive based Fabry-Pérot cavity combined with polymer fiber Bragg grating, Opt. Lasers Eng. **114** (2019)
10. F. Zhang *et al.*, Highly sensitive temperature sensor based on a polymer-infiltrated Mach-Zehnder interferometer created in graded index fiber, Opt. Lett. **44** (2019)
11. H. Chen *et al.*, Fiber-optic, extrinsic Fabry-Perot interferometric dual-cavity sensor interrogated by a dual-segment, low- coherence Fizeau interferometer for simultaneous measurements of pressure and temperature, Opt. Express **27** (2019)
12. G. Zhang, M. Yang, and M. Wang, Large temperature sensitivity of fiber-optic extrinsic Fabry-Perot interferometer based on polymer-filled glass capillary, Opt. Fiber Technol **19** (2013) 618

13. B. Li *et al.*, High-sensitivity temperature sensor based on ultraviolet glue-filled silica capillary tube, J. Mod. Opt. **67** (2020) 1327-1333
14. Z. J. Liu *et al.*, An Optical Microfiber Taper Magnetic Field Sensor With Temperature Compensation, IEEE Sens. J. **15** (2015) 4853-4856
15. Y. Liu *et al.*, High-Sensitive Temperature Sensor Based on Cascaded Polymer-Air Cavities, IEEE Photonics Technol. Lett. **33** (2021) 711-714
16. Y. Liu *et al.*, High-Sensitivity Temperature Sensor Based on Photosensitive Polymer-Filled Silica Capillary Tube, IEEE Photonics Technol. Lett. 32 (2020) 1461-1464
17. N. Liao *et al.*, sensitivity-enhanced micro-cavity extrinsic Fabry-Perot interferometric fiber-optic curvature sensor, Optik (Stuttg) **221** (2020)
18. Z. Ma *et al.*, Sensitivity-enhanced extrinsic fabry-perot interferometric fiber-optic microcavity strain sensor, Sensors (Switzerland) **19** (2019)
19. D. Jauregui *et al.*, Bitapered fiber sensor: Signal analysis, Sensors Actuators B Chem. **218** (2015)
20. X. Fu *et al.*, Phase demodulation of interferometric fiber sensor based on fast Fourier analysis, Opt. Express. **25** (2017)
21. E. Hecht, Optics (Pearson Education, 2016).
22. K. C. Yee and R. R. Chance, Synthesis and properties of a new polydiacetylene: Poly[1,6-di(N-carbazolyl)-2,4-hexadiyne], J. Polym. Sci. Polym. Phys. Ed. **16** (1978) 431-441
23. Y. Zhao *et al.*, Optical fiber Fabry-Perot humidity sensor based on polyimide membrane: Sensitivity and adsorption kinetics, Sensors and Actuators A Phys. **281** (2018) 48-54
24. Y. Yu *et al.*, Enhancing the pressure sensitivity of a Fabry-Perot interferometer using a simplified hollow-core photonic crystal fiber with a microchannel, Appl. Phys. B. **120** (2015) 461
25. Y. Li *et al.*, Optical hydrogen sensor based on PDMS-formed double-C type cavities with embedded Pt-loaded WO3/SiO2, Sensors Actuators B Chem. **276** (2018) 23-30
26. L. G. Abbas *et al.*, Highly sensitive polymer based fabryperot interferometer for temperature sensing, Prog. Electromagn. Res. Lett. **97** (2021) 87-94
27. J. Li, Y. n. Wang, and J. t. Yang, Compact Fabry-Perot microfiber interferometer temperature probe with closed end face, J. Int. Meas. Confed. **178** (2021)
28. G. Zhang, M. Yang, and M. Wang, Large temperature sensitivity of fiber-optic extrinsic Fabry-Perot interferometer based on polymer-filled glass capillary, Opt. Fiber Technol **19** (2013) 618-622
29. C. Dong *et al.*, Evaluation of thermal expansion coefficient of carbon fiber reinforced composites using electronic speckle interferometry, Opt. Fiber Technol **26** (2018)
30. M. D. Garcia *et al.*, Bi-tapered fiber sensor using visible to near infrared light **263** (2017) 285-290